ORIENTAL JOURNAL OF CHEMISTRY
An International Open Access, Peer Reviewed Research Journal
www.orientjchem.org
ISSN: 0970-020 X
CODEN: OJCHEG
2024, Vol. 40, No.(5):
Pg. 1232-1239

Adsorption of Amoxicillin using Oxidized Carbon Nanotubes of Aqueous Solution

ALIREZA FALAHATI MARVAST[1], ALI KHANZADEH POSHTIRI[2], FARNAZ DONIAMALI[3], ALIREZA SAEGH[4], DAVOUD BALARAK*[5] and SHAZIYA HASEEB SIDDIQUI[6]

[1]Department of Toxicology and Pharmacology, School of Pharmacy and Pharmaceutical Sciences, Shahid Sadoughi University of Medical Sciences, Yazd, Iran.
[2]Department of Natural Science, Gorgan University of agriculture and natural science, Gorgan, Iran.
[3]Department chemistry, PNU University Qazvin, Qazvin, Iran.
[4]Department of Pharmacy, Shahid Sadoughi University of Medical Sciences, Yazd, Iran.
[5]Department of Environmental Health, Health Promotion Research Center, Zahedan University of Medical Sciences, Zahedan, Iran.
[6]Department of Chemistry, Sam Higginbottom University of Agriculture Technology and Sciences (SHUATS), Allahabad, Uttar Pradesh, India.
*Corresponding authors E-mail: dbalarak2@gmail.com

http://dx.doi.org/10.13005/ojc/400504

(Received: August 05, 2024; Accepted: September 30, 2024)

ABSTRACT

The extensive therapeutic repertoire of antibiotics for both humans and animals has resulted in the direct or indirect release of these compounds into the environment, particularly into water ecosystems. Traditional methods for eliminating antibiotic residue from wastewater have proven to be largely ineffective, leading to a need for alternative treatments. As a result, there has been a significant increase in the attention given to other methods of antibiotic residue elimination. This paper presents the kinetic adsorption of Amoxicillin (AMX) onto Oxidized multiwalled Carbon Nanotubes (OMWCNTs). In the batch adsorption experiments, the focus was on exploring how initial concentration, temperature variations, and contact time affect the percentage of removal. Optimization strategies were then implemented to maximize the AMX adsorption capacity concurrently. A maximum of 98.71% AMX was removed at an optimum contact time 75 min and temperature 40. The rise in temperature led to an increase in adsorption capacity, signifying the endothermic nature of the adsorption reaction of AMX onto OMWCNTs, as observed in this study. When compared with other kinetic models, the R^2 obtained using the PSO rate equation are markedly higher. Mechanisms such as electrostatic interactions, hydrophobic interactions, hydrogen bonding, and others facilitate antibiotic removal by OMWCNTs, providing technical backing for antibiotic wastewater treatment.

Keywords: Adsorption, Oxidized carbon nanotubes, Amoxicillin, Thermodynamics, Kinetics.

INTRODUCTION

The widespread use of antibiotics has become a major concern due to their negative effects on both health and the environment[1,2]. Studies have shown the detection of antibiotics in various aquatic environments and water supplies. In most cases, these antibiotics exist as mixtures rather than individual compounds[3,4]. Even at low levels, the persistence of antibiotics in water bodies can promote the emergence of antibiotic-resistant genes and harm aquatic organisms, leading to ecosystem disruption and potential threats to human health[5]. Therefore, the development of efficient methods for the removal of antibiotics from aquatic environments is imperative[6,7].

A variety of techniques have recently been explored for wastewater treatment, including biodegradation, adsorption, ion exchange, membrane separation methods, and catalytic oxidation, all aimed at degrading and eliminating antibiotics[8,9]. Among these techniques, adsorption processes offer a promising approach for eliminating antibiotics due to their efficiency, simplicity, flexibility, and cost-effectiveness[10]. Effective water purification and antibiotic removal require adsorbents with high adsorption capacity and specific selectivity, attributes typically found in porous adsorbents with large pore diameters and abundant functional groups such as -OH and -COOH[11,12]. However, the adsorption of large-molecule antibiotics from aqueous solutions by adsorbents with smaller pore sizes is hindered by the size exclusion effect. Additionally, the presence of numerous functional groups on material surfaces enhances antibiotic removal from wastewater[13,14]. Mesoporous carbon, with its and abundant functional groups, high surface area, and large pore volume, emerges as a promising candidate for adsorbing large-molecule contaminants[15,16].

The limited biodegradability of antibiotics renders conventional biological treatment processes relatively ineffective in treating antibiotic manufacturing wastewater[17,18]. Consequently, physical or chemical treatments are often favored. Nonetheless, these methods can be costly and may not adequately address the broad spectrum of antibiotic wastewaters[19,20]. AC serves as a popular adsorbent for antibiotic removal through adsorption[21]. Nevertheless, the expensive nature of AC has driven the exploration and adoption of numerous alternative adsorbents for removing antibiotics from aqueous solutions[22,23].

Ever since their discovery, CNTs have been extensively studied across various disciplines[24]. The vast potential for future engineering applications is indicated by the exceptional mechanical properties, remarkable electrical conductivity, small size, and large surface area of these materials[25,26]. Within the spectrum of CNTs, SWCNTs and MWCNTs are delineated based on the number of layers they exhibit[27]. The production approaches for MWCNTs are relatively straightforward and can be easily scaled up to accommodate large-scale production.

Carbon nanotubes (CNTs) are cylindrical structures composed of one or more rolled-up sheets of graphene. Oxidation refers to the process of introducing oxygen-containing functional groups (like carboxylic acid, hydroxyl, and carbonyl) onto the surface of CNTs. This chemical modification significantly alters their physical and chemical properties[20].

Pristine CNTs tend to aggregate due to strong van der Waals forces. Oxidation introduces polar groups, enhancing their solubility in polar solvents and improving dispersion, making them easier to process and integrate into composites. Functional groups introduced through oxidation increase CNT reactivity, enabling better adhesion to other materials and facilitating chemical modification for specific applications[21]. Oxidized CNTs exhibit increased wettability, making them suitable for applications involving contact with liquids, such as filtration and sensors. In some cases, oxidation can enhance the electrical conductivity of CNTs by creating defects that act as charge carriers[22]. In this study, we used oxidized carbon nanotubes to remove amoxicillin, which has not been used in other studies.

MATERIALS AND METHODS

The main chemical employed in our study, as the pollutant, was AMX prepared by Merck (Darmstadt, Germany). Fig. 1 illustrates the chemical structure of AMX. To adjust the pH of the solution, either 0.1 M H_2SO_4 or NaOH was used. Experiments were accomplished in conical flasks (250 mL), in batch mode.

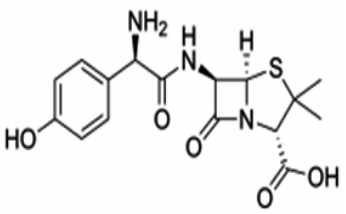

Fig. 1. Chemical structure of the used AMX

For the production of MWCNTs, chemical vapor deposition (CVD) of acetylene in a hydrogen atmosphere at 760°C was employed, with Ni–Fe nanoparticles serving as catalysts. $Fe(NO_3)_2$ and $Ni(NO_3)_2$ underwent a sol–gel process and subsequent calcination to obtain FeO and NiO, respectively. Fe and Ni nanoparticles were generated through deoxidation of the mentioned compounds using H_2. The ends of the tubes were uncapped by placing the raw MWCNTs in a liquid consisting of 3M HNO_3. We did this so we can use the MWCNTs for something else. We mixed 3 g of MWCNTs with 400 mL of 3 M HNO_3 and used sound waves to stir it for 24 hours. After that, we filtered the mixture and rinsed it with clean water until the liquid had a pH of about 6. Then, we dried the mixture at 80 degrees Celsius. Following this, the oxidized MWCNTs underwent a calcination process at 450°C for 24 h to eliminate any remaining amorphous carbon, after which they were utilized in the subsequent experiments. The experiments used chemicals that were of analytical purity and were directly employed without any additional purification steps. Additionally, Milli-Q water was utilized to prepare the solutions.

The experiments were fulfilled at ambient conditions and T = 28 ± 2°C; for this purpose, polyethylene tubes, as batch system, were employed. To conduct the measurements, a specific quantity of OMWCNT was mixed with AMX solution (this was done in 100 mL flasks) and shaken at a fixed rate of 200rpm for a certain period. Once the adsorption experiments were finished, an external magnet was used to separate the OMWCNT. UV-Vis spectroscopy was used to track changes in absorbance of AMX solution samples at specific time intervals. The maximum wavelengths (λ_{max}) of 622nm were utilized for the determination of the changes. The removal ratio (R%) of AMX was computed by comparing its initial and equilibrium concentrations. All the experimental results were obtained from duplicate determinations and had a relative error of roughly 5%.

The thermodynamic parameters, including the free energy change (ΔG^0), enthalpy change (ΔH^0), and entropy change (ΔS^0), were estimated using the equations presented below[20].

$$\Delta G^0 = -RT \ln (Kc) \quad (1)$$

$$\ln (K_c) = \frac{\Delta S^0}{R} - \frac{\Delta H^0}{RT} \quad (2)$$

Kc is the symbol used to represent the sorption equilibrium constant, R is the symbol used to represent the gas constant, and T is the symbol used to indicate the absolute temperature in Kelvin.

RESULTS AND DISCUSSION

Analysis using the N2-BET method revealed the specific surface area of the OMWCNTs to be 214 m^2/g. Subsequent examination of the OMWCNT morphologies was conducted via scanning electron microscopy (SEM) utilizing a JEOL JSM-6700F instrument (see Fig. 2). The SEM illustrates OMWCNTs characterized by exceptionally smooth surfaces, with diameters varying from 10 to 30nm and lengths measuring several micrometers.

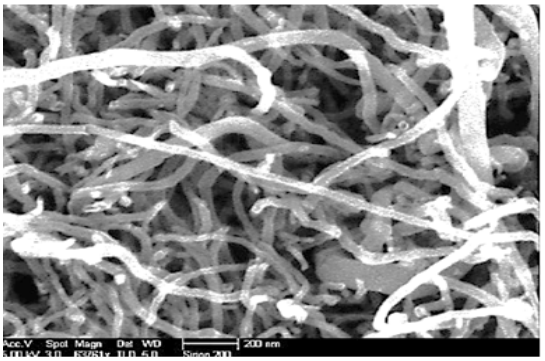

Fig. 2. SEM image of OMWCNTs sample

Effect of parameters on antibiotic adsorption

The design of cost-effective wastewater treatment systems relies heavily on determining the equilibrium time, which is a critical parameter. In order to study the adsorption kinetics, five distinct AMX quantities were selected. Fig. 3 illustrates the relationship between the adsorption capacity (q_t) of AMX onto OMWCNTs and contact time for different initial concentrations of AMX. The qt value showed a steep rise from 98.8 mg/g to 829.4 mg/g as the concentration rose from 10 mg/L to 100 mg/L, as seen in Figure 3.

The impact of the initial concentration of AMX on the adsorption process was studied by varying it from 10 to 100 mg/L. The pH was kept constant at 7, and the amount of adsorbent was fixed at 0.2 g/L. The contact time was set at 10-150 minute. According to Fig. 3, the efficiency of elimination reduced with the rise in the initial AMX concentration. The minimum efficiency was observed at an initial AMX concentration of 100 mg/L.

Adsorption process was also deliberated at four different temperatures to analyze its temperature dependence. The initial AMX concentrations were varied over a range, and the adsorption isotherms were used to analyze how changes in temperature affect the studied process. Fig. 4 illustrates the variation in adsorption isotherms with temperature. The experimental results indicated an enhancement in the equilibrium uptake by rising the equilibrium AMX concentrations within the experimental concentration range.

To investigate the kinetic behavior of AMX adsorption onto OMWCNTs, three commonly used kinetic models were employed, namely the PFO, PSO, IPD model. In PSO model, the rate-limiting step is the surface adsorption that involves chemisorption, where the removal from a solution is due to physicochemical interactions between the two phases[27]. The model that best fit the data was designated based on the correlation coefficient values(R^2) obtained through linear regression. Equation 3 represents the PFO model[28,29].

$$\text{Log}\,(q_e - q_t) = \log q_e - \frac{K_1}{2.303}t \qquad (3)$$

The quantities of AMX adsorbed at equilibrium and time t are represented by qe and q_t (mg/g), respectively. The rate constant of the PFO is denoted by k_1 (min^{-1}). The slope and intercept of the $\log(q_e\text{-}q_t)$ versus t plots can be employed to compute the values of k_1 and q_e. These calculations are presented in Fig. 5a. The R^2 gotten for all considered concentrations are in the range of 0.75-0.85 and are low. Additionally, the $q_{e,exp}$ (mg/g) experimental values are significantly different from the calculated $q_{e,cal}$ (mg/g). As a result, the PFO does not effectively describe the adsorption process.

Equation 4 expresses a PSO in a linear form[30,31].

$$\frac{t}{q_t} = \frac{1}{k_2 qe^2} + \frac{t}{qe} \qquad (4)$$

The PSO rate constant, k_2 (g/mg min), can be derived from the rate equation. The values of q_e and k_2 can be obtained by plotting t/q_t against t (Fig. 5b). The high R^2 (>0.999) of the linear plots at different concentrations indicate that the adsorption of AMX onto OMWCNTs follows the PSO predominantly. Besides, the qe,cal are in good agreement with the $q_{e,exp}$. Table 1 summarizes the equations related to kinetic models and the results obtained from their application.

The two aforementioned models are unable to determine the diffusion mechanism that occurs during the studied process. Therefore, the experimental data is examined using the IPD model (equation 5)[32,33].

$$q_t = K_d\, t^{0.5} + C \qquad (5)$$

In above equation, kd (mg/g $min^{1/2}$) signifies the IPD rate constant, and C is the intercept. The adsorption mechanism of a solute from a solution onto porous adsorbents progresses through three distinct phases. Following this, the process transitions into a stage of gradual adsorption (step II), where the rate-limiting factor becomes IPD. Finally, equilibrium is achieved, with IPD slowing down caused by the minimal concentrations of adsorbate left in the solutions[34]. The regulation of the adsorption rate is influenced by one or more of these three stages.

In the graph depicted in Fig. 5c, where q_t is plotted against $t^{1/2}$, a dual linear trend is observed. Initially, it is posited that AMX quickly migrates to the outer surface of OMWCNTs via film diffusion within a short duration. The initial linear phase likely reflects the penetration of AMX molecules into the OMWCNTs particle through IPD. Subsequently, the subsequent linear portion signifies the establishment of final equilibrium[35].

Over the past few years, the identification of human medicines and pharmaceutical drugs in sewage, wastewater, and domestic water systems has brought attention to their potential ecotoxicological effects on human health in numerous countries[36]. The detrimental impacts of pharmaceuticals in water resources pose serious risks to human health, as well as to animals and plants, with far-reaching consequences[37].

The data presented in Fig. 3 demonstrate a direct relationship between equilibrium uptake and increasing concentrations of AMX within the experimental concentration range. The explanation for this could lie in the enhanced driving force resulting from the concentration gradient. For

higher concentration of AMX, more AMX ions surrounded the active sites of OMWCNTs, facilitating adsorption and consequently leading to an increase in q_e values[38]. Additionally, it was noted that the q_e rose with increasing temperature, suggesting the endothermic nature of AMX adsorption onto OMWCNTs[39,40]. It's feasible that this arises from the strengthening of physical bonding between AMX molecules and the active sites of the adsorbent at higher temperatures, coupled with the increased solubility of AMX, which enhances interaction forces between the solvent and the solute[41].

The concentration of the pollutant (AMX) at the start of the study is a critical factor in adsorption and requires assessment. Previous research has demonstrated significant effects of this factor up to a certain limit. Additionally, the adsorption capacity of the adsorbent for AMX molecules depends on the presence of sorption sites on its surface. Once the optimal value is exceeded, the adsorption efficiency decreases due to the saturation of active sites on the adsorbent's surface[35]. Moreover, there is minimal available space between the layers of OMWCNTs, and the adsorption process involves replacing interlayer anions of the adsorbent with contaminants. This space can accommodate the ideal values of OMWCNTs and enable efficient adsorption[40]. Consequently, the saturation of active sites in the interlayer of OMWCNTs prevents further diffusion of contaminants onto the adsorbent.

The concentration of AMX during initial stages significantly impacts its adsorption capacity on OMWCNTs adsorbent. The observation reveals that as the initial AMX concentration increases, the adsorption capacity of AMX also increases. A heightened driving force of the concentration gradient with the increase in the initial concentration could be the reason behind this phenomenon. During the initial stages of adsorption (contact time<45 min), the process is rapid, whereas it slows down later on. The presence of many vacant surface sites at the outset may contribute to this, making it easier for AMX molecules to adsorb. However, as the surface sites get occupied, the unoccupied sites become challenging to fill due to repulsive forces between the AMX molecules on the OMWCNTs and the bulk phase[34]. The curves observed during the process are single, smooth, and continuous towards saturation, signifying that monolayer coverage of AMX molecules on OMWCNTs surface has been achieved[35].

The thermodynamic parameters provide valuable information such as the strength of adsorbate attachment to the adsorbent surface, whether the process is chemisorption or physisorption, whether it is exothermic or endothermic, and the entropic changes during adsorption. Physisorption occurs when the $\Delta G°$ value is approximately 20 kJ/mol, while chemisorption occurs when the value ranges from 80-400 kJ/mol[33]. According to the results of the adsorption model, the adsorption of the drug on the OMWCNTs adsorbent was determined to be physisorption. A negative $\Delta G°$ value designates that the adsorption is endothermic and spontaneous. It was observed that the change in free energy decreases with increasing temperature, but the nature of adsorption is non-normal. It is possible that the reason for this is the strengthening of the adsorption process caused by rising temperature[35]. The $\Delta G°$ for AMX adsorption was found to be within the range of -2.2 to -8.9 kJ/mol, indicating that the adsorption was primarily physical adsorption[36]. A $\Delta S°>0$ specifies a developed randomness between solid-solution interfaces during the adsorption of AMX on OMWCNTs[38].

The graph in Fig. 5c illustrates the plot between q_t and $t^{0.5}$ for AMX adsorption and desorption onto OMWCNTs. It is evident from the graph that both adsorption and desorption exhibit a multi-linear behavior, with two distinct steps visible in the plots representing the initial and second stages[36]. The initial stage is likely associated with the boundary layer diffusion effect, while the next stage may be a result of IPD effects. The current study revealed that the rate constants (k_d) governing both adsorption and desorption exhibit higher magnitudes, showing an upward trend with increasing initial AMX concentration. Consequently, the linear section at the upper portion of the graph can be interpreted as a rate parameter (k_d), indicative of the adsorption and desorption rates within the domain where IPD was identified as the rate-controlling step[34].

Table 2 shows a comparison of the adsorption capacity (q_e) of different materials reported in the articles as adsorbent for AMX adsorption from aqueous solution under different experimental conditions.

The mechanism of adsorption of AMX to the OMWCNTs material involves a multi-step process where molecules move into the material. This process is seen in the data as a steep part (bulk

diffusion) followed by a less steep part (film and pore diffusion)[35].

Additionally, the OMWCNTs surface has different chemical features like -OH and -C=O groups that can bind to AMX in various ways, including strong (covalent) and weak (hydrogen bonding, ionic interaction, etc.) connections. The -NH_2 groups can also bond with AMX through strong (imine) and weaker (amide) connections, and other interactions Figure 6.

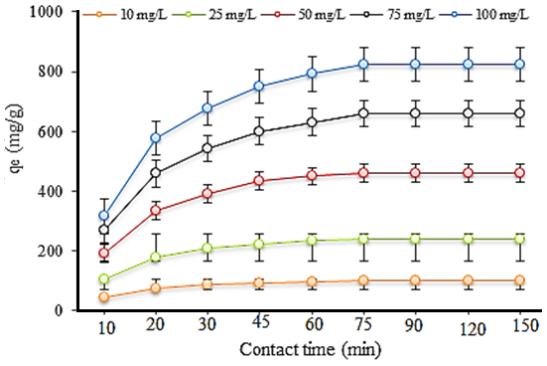

Fig. 3. Effect of contact time (temperature: 303 K, adsorbent dose: 0.1 g/L)

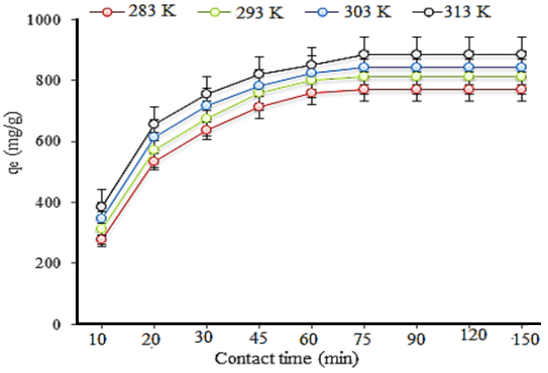

Fig. 4. Effect of temperature (C0:100 mg/L, adsorbent dose: dose: 0.1 g/L, time: 75 min)

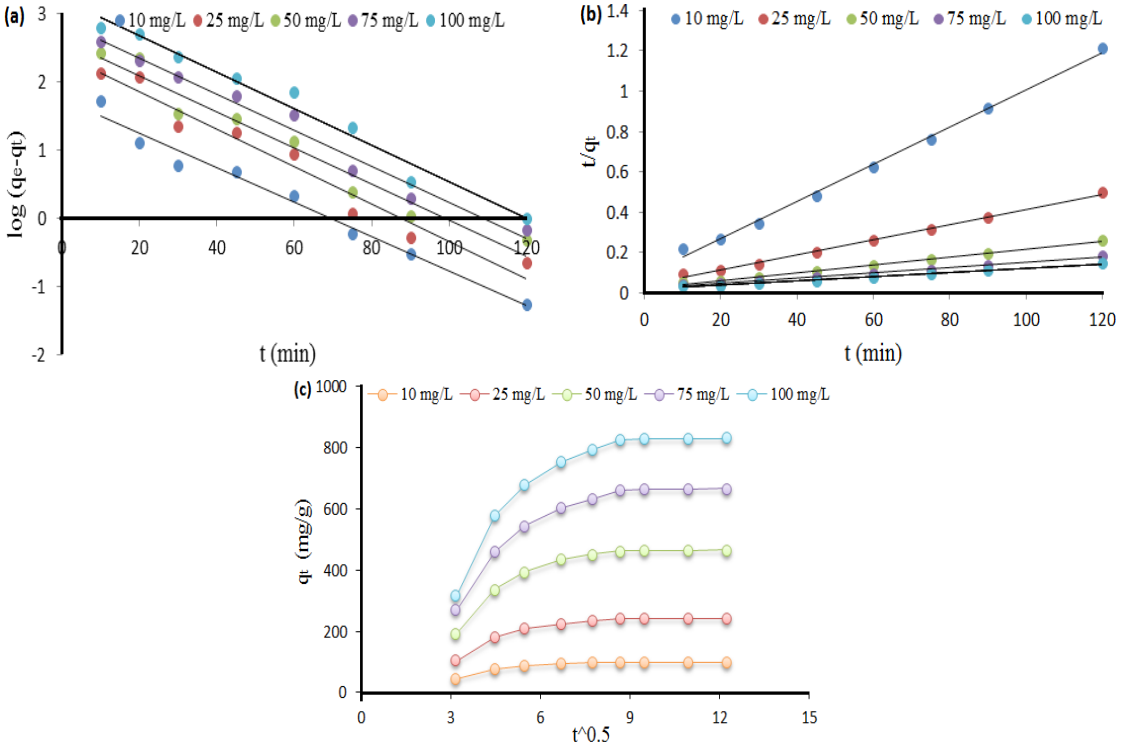

Fig. 5. PFO (a); PSO (b); IPD (C); kinetic plots for AMX adsorption onto OMWCNTs

Table 1: Values of kinetic parameters for the adsorption of AMX

AMX (mg/L)	$(q_e)_{exp}$	IPD model			PFO			PSO		
		K_d	I	R^2	$(q_e)_{cal}$	K_1	R^2	$(q_e)_{cal}$	K_2	R^2
10	41.55	2.11	11.62	0.752	11.6	0.451	0.895	21.2	0.004	0.997
25	81.34	3.65	25.47	0.787	19.47	0.274	0.912	65.2	0.001	0.996
50	119.1	7.94	29.76	0.884	28.94	0.011	0.904	161.2	0.0009	0.994
75	155.1	10.25	38.48	0.816	59.73	0.046	0.876	214.2	0.0004	0.998
100	196.1	14.2	44.3	0.793	67.2	0.074	0.871	251.7	0.0007	0.992

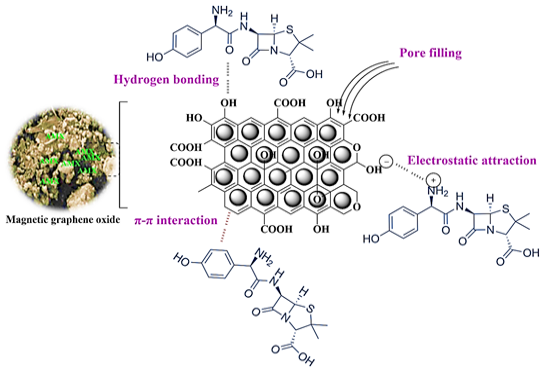

Fig. 6. Adsorption mechanism of AMX onto OMWCNTs

Table 2: Comparison of the maximum adsorption of various adsorbent for AMX

Adsorbents	Q_e(mg/g)	Reference
AC- Jujube nuts	56.2	13
MWCNT	465.1	14
AC- cashew of Para	56.95	15
AC-Date Pits	84.93	18
AC-olive stone	84.1	21
Synthesized NiO	94.3	26
Magnetic graphene oxide	93.2	34
OMWCNTs	926.2	This study

CONCLUSION

In the present investigation, it was found that the adsorbent demonstrated a maximum uptake capacity of 829.4 mg/g and achieved a total percentage removal of 98.71% of AMX from the aqueous solution. Optimal physicochemical parameters were determined to be a dosage of 0.1 g, a contact time of 75 min, and a temperature of 40°C, respectively. Various adsorption kinetic models, including the PFO, PSO, and IPD models, were employed to assess the kinetics of maltose sorption by OMWCNTs. The results indicate that the sorption of AMX onto OMWCNTs conforms well to the PSO.

ACKNOWLEDGEMENT

The authors are grateful to Zahedan University of Medical Sciences, because of supporting this research (IR.ZAUMS.REC.1400.379).

Conflicts of interest

The authors declare no conflict of interest.

REFERENCES

1. Fei Y.; Li Y.; Han S.; Ma J., *J. Colloid Interface Sci.*, **2016**, *484*, 196–204.
2. Balarak D.; Mahvi AH.; Shim MJ.; Lee SM., *Desalin Water Treat.*, **2021**, *212*, 390-400.
3. Ahmadi S.; Banach A.; Mostafapour FK., *Desalin Water Treat.*, **2017**, *89*, 297-303.
4. Yilmaz M.; Al-Musawi TJ.; Saloot MK., *Biomass Conv. Bioref.*, **2022**. https://doi.org/10.1007/s13399-021-02279-y
5. Al-Musawi TJ.; Mengelizadeh N.; Taghavi M., *Biomass Conv. Bioref.*, **2021**. https://doi.org/10.1007/s13399-021-01962.
6. Wang H.; Fang C.; Wang Q.; Chu Y.; Song Y.; Chen Y.; Xue X., *RSC Adv.*, **2018**, *8*, 16260–16268.
7. Wang J.; Zhang M.; Zhou R.; Li J.; Zhao W.; Zhou J., *Water Sci Technol.*, **2020**, *82*, 242–254.
8. Wu S.; Hu YH., *Chem Eng J.*, **2021**, *409*, 127739.
9. Mahvi AH.; Mostafapour FK., *Fresenius Environ Bull.*, **2018**, *27*(8), 5759-67.
10. Balarak D.; Taheri Z.; Shim MJ.; Lee SM.; Jeon C., *Desalin Water Treat.*, **2021**, *215*, 183-193.
11. Azarpira H.; Mahdavi Y.; Khaleghi O., *Pharm Lett.*, **2016**, *8*(11), 107-13.
12. Shikuku VO.; Zanella.; Kowenje CO., *Appl Water Sci.*, **2018**, *8*, 175. https://doi.org/10.1007/s13201-018-0825-4.
13. Belaissa, Y.; Saib, F. & Trari, M., *Reac Kinet Mech Cat.*, **2022**, *135*, 1011–1030.
14. Balarak D.; Mostafapour FK.; Bazrafshan E.; Saleh T. A., *Water Sci Technol.*, **2017**, *75*, 1599-1606.
15. Lima, DR.; Lima, EC.; Umpierres, C. S., *Environ Sci Pollut Res.*, **2019**, *26*, 16396–16408. https://doi.org/10.1007/s11356-019-04994-6.
16. Leonard JM. Githinji, MKM., Ramble O. Ankumah., *Water Air Soil Pollutant.*, **2011**. *2019*, 191-201.
17. Ibáneza M.; Bijlsmaa L.; Moralesb E.; Pastorb L, Hernándeza F., *J. Hazard. Mater.*, **2013**. *260*, 389-398.
18. Belhachemi, M.; Djelaila, S., *Environ. Process.*, **2017**, *4*, 549–561.
19. Boukhelkhal, A.; Benkortbi, O.; Hamadeche, M., *Water Air Soil Pollut.*, **2015**, *226*, 323. https://doi.org/10.1007/s11270-015-2587-z.
20. Moarefian, A.; Golestani, H. A. & Bahmanpour, H., *J Environ Health Sci Eng.*, **2014**, *12*, 127. https://doi.org/10.1186/s40201-014-0127-1.

21. Limousy, L.; Ghouma, I.; Ouederni, A., *Environ Sci Pollut Res.*, **2017**, *24*, 9993–10004. https://doi.org/10.1007/s11356-016-7404-8.
22. Gao H.; Zhao S.; Cheng X.; Wang X.; Zheng L., *Chem. Eng. J.*, **2013**, *223*, 84–90.
23. Balarak D.; Mostafapour FK.; Joghataei A., *Pharm. Chem.*, **2016**, *8*(8), 138-145.
24. Balarak D.; Mahdavi Y.; Bazrafshan E.; Mahvi AH.; Esfandyari Y., *Fluoride.*, **2016**, *49*(1), 71-83.
26. Naghsh N.; Chandrika K.; Balarak D., *Int. J. Pharm. Investigation.*, **2024**, *14*(2), 365-70.
27. Eltaweil AS.; Abd El-Monaem EM., El-Subruiti GM., *J Porous Mater.*, **2023**, *30*, 607–618.
28. Balarak D.; Chandrika K., *Int J Pharm Investig.*, **2019**, *9*(3), 117-21.
29. Rout.; DR.; Jena.; HM., *Environ Sci Pollut Res.*, **2022**, *29*, 32105–32119. https://doi.org/10.1007/s11356-021-17944-y.
30. Mostafapour FK.; Bazi M.; Siddiqui SH.; Bagheri H., *Int J Pharm Investig.*, **2021**, *11*(4), 384-8.
31. El Rouby WMA.; Farghali AA.; Sadek MA., *J Inorg Organomet Polym.*, **2018**, *28*, 2336–2349. https://doi.org/10.1007/s10904-018-0885-9.
32. Li R.; Wang Z.; Zhao X., *Environ Sci Pollut Res.*, **2018**, *25*, 31136–31148. https://doi.org/10.1007/s11356-018-3064-1.
33. Balarak D.; Ganji F.; Chandrika K.; Haseeb S., *Int J Pharm Investig.*, **2020**, *10*(2), 122-6.
34. Mostafapour FK.; Haseeb S.; Balarak D.; Moein H.; Sajadi AA.; Jalalzaei Z., *Int J Pharm Investig.*, **2021**, *11*(1), 41-5.
35. Kong X.; Liu Y.; Pi J., *Environ Sci Pollut Res.*, **2017**, *24*, 6679–6687.
36. Liang, H.; Zhu, C.; Ji, S., *Biochar.*, **2022**, *4*, 3. https://doi.org/10.1007/ s42773-021-00130-1.
37. Shan DN.; Deng SB.; Zhao TN.; Wang B.; Wang YJ.; Huang J.; Yu G.; Winglee J.; Wiesner MR., *J Hazard Mater.*, **2016**, *305*, 156–163.
38. Zisti F.; Chandrika K., *Int. J. Pharm. Investigation.*, **2023**, *13*(4), 778-83.
39. Azadfar M.; Tahermansouri H.; Qomi M., *J. Chin. Chem. Soc.*, **2021**, *68*, 2103–2117.
40. Gholizadeh, H.; Ghorbani-HasanSaraei A.; Tahermansouri H., *Carbon Lett.*, **2019**, *29*, 273–279.
41. Gholizadeh, H.; Ghorbani-HasanSaraei A.; Tahermansouri H. Shahidi SA., *J. Chin. Chem. Soc.*, **2020**, *67*, 546–557.